Supplementary Information

Kinetic and deuterium isotope analyses of ammonia electrochemical synthesis

Authors: Chien-I Li,[a] Hiroki Matsuo[b] and Junichiro Otomo*[b]

Affiliations and addresses:

[a]*Department of Environment Systems,*
Graduate School of Frontier Sciences,
The University of Tokyo,
5-1-5 Kashiwanoha, Kashiwa-shi, Chiba 277-8563, Japan

[b]*Department of Transdisciplinary Science and Engineering,*
School of Environment and Society,
Tokyo Institute of Technology,
2-12-1 Ookayama, Meguro-ku, Tokyo 152-8550, Japan.

* Corresponding author:

E-mail correspondence: otomo.j.aa@m.titech.ac.jp

1. Electrode potential

$$\text{Electrode potential} = V_{app} - (IR_{ohm} + \frac{RT}{nF}\ln(p_{H2,\,anode}/p_{H2,\,1bar})) \quad \text{(S1)}$$

The electrode potential is described as following equation:

,

where V_{app}, I, R_{ohm}, R, T, n, F, p_{H2}, anode, are applied voltage, current, ohmic resistance, gas constant, temperature, electron transfer number, Faraday constant, H_2 partial pressure in the anode, respectively. IR_{ohm} is IR loss correction. $\frac{RT}{nF}\ln(p_{H2,\,anode}/p_{H2,\,1bar})$ is a correction of the potential difference between the H_2 partial pressure in reference electrode and 1 bar H_2 pressure.

Table S1 Electrode potential calculated by Eq. S1 at different H_2 partial pressures.

Applied Voltage (V)	Electrode potential (V)				
	5% H_2−50% N_2−45% Ar	10% H_2−50% N_2−40% Ar	15% H_2−50% N_2−35% Ar	20% H_2−50% N_2−30% Ar	25% H_2−50% N_2−25% Ar
Rest potential	0.087	0.065	0.055	0.04	0.027
−0.3	−0.024	−0.043	−0.04	−0.046	−0.052
−0.7	−0.126	−0.169	−0.157	−0.098	−0.132
−1	−0.241	−0.318	−0.363	−0.233	−0.241
−1.3	−0.389	−0.437	−0.537	−0.332	−0.383

2. Reaction order (β) of nitrogen

As shown in Fig. S1, the ammonia formation rate was investigated in H_2−N_2 gaseous mixtures with fixed H_2 partial pressure of 0.1 atm and with changing N_2 partial pressures of 0.3−0.6 atm (i.e., Ar was added to control H_2 and N_2 concentrations). The corresponding ammonia partial pressure was estimated in section 3 in the supplementary information. The ammonia formation rate showed a slight increase when N_2 partial pressure was increased. The effect of an increase in N_2 partial pressure on ammonia formation rate was not significant in comparison with that of an increase in H_2 partial pressure. The reaction order of nitrogen, β, was 0.3 at rest potential. After applying the different voltages, β were between 0.37 and 0.59. Current densities were almost the same at different N_2 partial pressures. The corresponding electrode potentials were shown in Table S2.

Table S2 Electrode potential calculated by Eq. S1 at different N_2 partial pressures.

Applied Voltage (V)	Electrode potential (V)			
	10% H_2−30% N_2−60% Ar	10% H_2−40% N_2−50% Ar	10% H_2−50% N_2−40% Ar	10% H_2−60% N_2−30% Ar
Rest potential	0.058	0.065	0.065	0.067
−0.3	−0.021	−0.034	−0.043	−0.037
−0.7	−0.026	−0.049	−0.169	−0.117
−1	−0.064	−0.097	−0.318	−0.159
−1.3	−0.284	−0.237	−0.437	−0.348

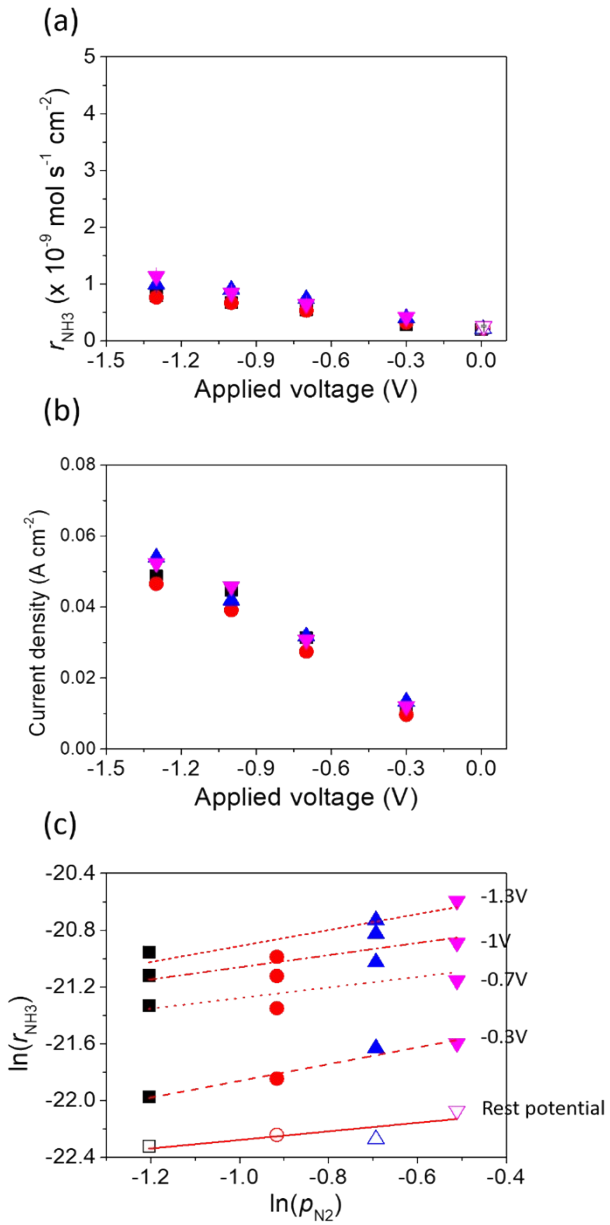

Fig. S1 (a) Ammonia formation rate, (b) current density, and (c) ln(r_{NH3}) vs. ln(p_{N2}) using porous pure Fe cathode at 550°C and different N_2 partial pressures. ● 10% H_2−30% N_2 with cathodic polarization. ● 10% H_2−30% N_2 at the rest potential. ∞ 10% H_2−40% N_2 with cathodic polarization. ∞ 10% H_2−40% N_2 at the rest potential. ■ 10% H_2−50% N_2 with cathodic polarization. ❒ 10% H_2−50% N_2 at the rest potential. ❑ 10% H_2−60% N_2 with cathodic polarization. ♦ 10% H_2−60% N_2 at the rest potential.

3. Ammonia partial pressure

The ammonia formation rate was 3.77×10^{-9} at −1.3 V and 550°C in 25% H_2−50% N_2−25% Ar. The total ammonia partial pressure could be obtained by the following equation:

$$p_{total} = \frac{r_{NH3} \times A \times R \times T}{\upsilon} \quad \text{(S2)}$$

where A, R, T, and υ were the electrode area of cathode, gas constant, temperature, and flow rate in the cathode.

4. v_2 band for NH_3

The energy level splitting between symmetric state (s) and asymmetric state (a) in NH_3 is due to the barrier of umbrella inversion for nitrogen atom travels through the three hydrogen atoms plane, as shown in Fig. S2.[1] The existence of the barrier resulting in a doubling of each vibrational-energy level is not excessive, so the molecule can tunnel through the planar state and flip between the two conformations. The vibrational-rotational transition in v_2 band were shown in Fig. S3.

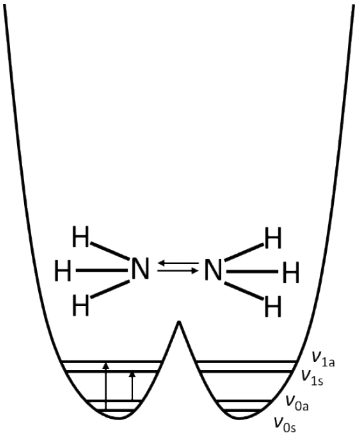

Fig. S2 Energy level splitting for the ground state and the first excited state of vibration.

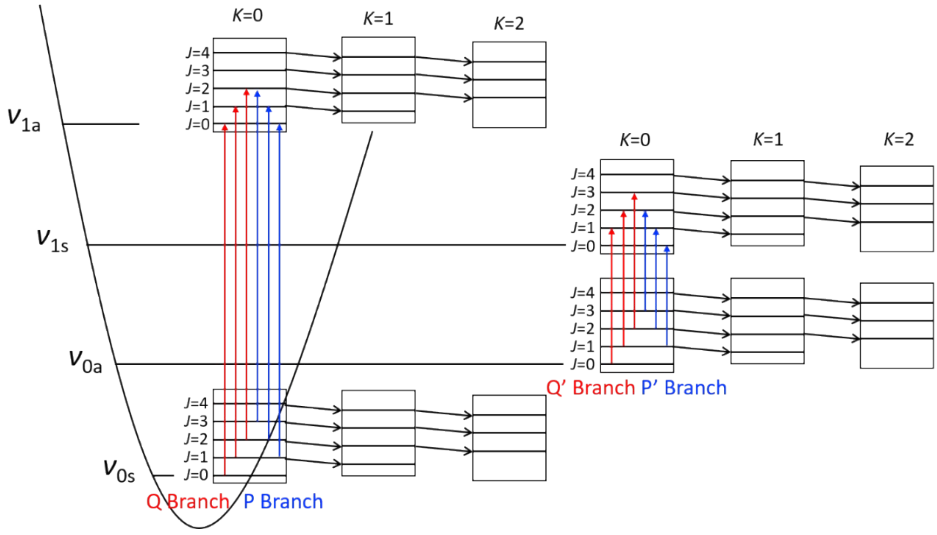

Fig. S3 Transition of Q and P branches for the v_2 vibration. Q and Q' represent the transition from symmetric state (s) to asymmetric state (a) and asymmetric state (a) to symmetric state (s), respectively, as $J = 0$. P and P' represent the transition from symmetric state to asymmetric state and asymmetric state to symmetric state, respectively, as $J = -1$.

5. Vibration-rotational states for $NH_{3-x}D_x$

The Eq. S3 was used to calculate the vibrational-rotational energy levels, E.[2, 3] The parameters for $NH_{3-x}D_x$ were summarized in Tables S3 and S4.

$$E = v + 1/2(A + B) \times [J \times (J + 1) - K^2] + C \rangle K^2 - D_K \times K^4 \quad \text{(S3)}$$

where J and K were total angular momentum and the projection of J onto the principal axis of the molecule, respectively.

Table S3 Parameters used in NH_3 and NH_2D (cm^{-1}).[2, 3]

	NH_3				NH_2D			
	Ground state		$v_2 = 1$		Ground state		$v_2 = 1$	
	Symmetry state (s)	Asymmetry state (a)	Symmetry state (s)	Asymmetry state (a)	Symmetry state (s)	Asymmetry state (a)	Symmetry state (s)	Asymmetry state (a)
v	0	0.793	932.434	968.122	0	0.406	876.374	896.562
A	9.947	9.9415	10.07	9.89	9.678	9.674	9.827	9.699
B	9.947	9.9415	10.07	9.89	6.411	6.41	6.408	6.359
C	6.227	6.228553	6.087	6.159	4.696	4.697	4.618	4.649
D_J	0.000849	0.000832	0.001131	0.000697	0.000527	0.000521	0.0006628	0.000466
D_{JK}	−0.001578	−0.00153	−0.00242	−0.00123	−0.0008	−0.0007852	−0.0010441	−0.0007
D_K	0.0010107	0.000979	0.001617	0.000811	0.000365	0.0003579	0.0004802	0.000311

Table S4 Parameters used in NHD_2 and ND_3 (cm^{-1}).[4, 5]

	NHD_2				ND_3			
	Ground state		$v_2 = 1$		Ground state		$v_2 = 1$	
	Symmetry state (s)	Asymmetry state (a)	Symmetry state (s)	Asymmetry state (a)	Symmetry state (s)	Asymmetry state (a)	Symmetry state (s)	Asymmetry state (a)
v	0	0.171	810.227	819.565	0	0.053	745.597	749.1448
A	5.344	5.344	5.312	5.296	5.143	5.1428265	5.224	5.216
B	7.446	7.445	7.529	7.48	5.143	5.1428265	5.224	5.216
C	3.753	3.753	3.705	3.718	3.124	3.12408768	3.088	3.094
D_J	0.000332	0.0003304	0.0003766	0.000312	0.000197	0.00019651	0.0002306	0.000219
D_{JK}	−0.00045	−0.0004463	−0.0006086	−0.00043	−0.00035	−0.00034794	−0.0004162	−0.00038
D_K	0.000157	0.000156	0.0003079	0.000187	0	−6.3944E-07	−0.0000382	0.000008

Table S5–S8 showed Q, P, and R branches for $NH_{3-x}D_x$ v_2 band. i and i' (i = R, P, and Q) represented the wavenumber from symmetric state (s) to asymmetric state (a) and from asymmetric state (a) to symmetric state (s), respectively.

Table S5 Q, P, and R branches for NH_3 v_2 band.

R branch at $K = 0$ (cm^{-1})			P branch at $K = 0$ (cm^{-1})			Q branch (cm^{-1})		
J	R	R'	*J*	P	P'	*J*	Q	Q'
0	987.8992	951.7765	1	948.2314	911.7613	1	967.9971	931.6279
1	1007.546	972.1406	2	928.2478	892.1574	2	967.7364	931.3322
2	1027.05	993.4597	3	908.1952	872.8421	3	967.3398	930.754
3	1046.401	1013.41	4	888.1012	853.821	4	966.8076	929.8922
4	1065.594	1034.226	5	867.9973	835.0926	5	966.1401	928.7447
5	1084.627	1055.09	6	847.9183	816.6481	6	965.3378	927.3083

Table S6 Q, P, and R branches for NH_2D v_2 band.

R branch at $K = 0$ (cm^{-1})			P branch at $K = 0$ (cm^{-1})			Q branch (cm^{-1})		
J	R	R'	*J*	P	P'	*J*	Q	Q'
0	912.6181	892.2003	1	880.4751	859.8861	1	896.4996	875.9643
1	928.6323	908.5672	2	864.3701	843.9671	2	896.3436	875.8022
2	944.5949	925.4405	3	848.2611	828.2202	3	896.0947	875.4811
3	960.4975	941.6239	4	832.1638	812.651	4	895.7539	875.0008
4	976.3333	958.2649	5	816.0951	797.2618	5	895.3223	874.3606
5	992.0972	974.9427	6	800.0736	782.0515	6	894.8016	873.5598

Table S7 Q, P, and R branches for NHD_2 v_2 band.

R branch at $K = 0$ (cm^{-1})			P branch at $K = 0$ (cm^{-1})			Q branch (cm^{-1})		
J	R	R'	*J*	P	P'	*J*	Q	Q'
0	832.3398	822.8955	1	806.7763	797.2683	1	819.523	810.034
1	845.0931	835.7778	2	793.9817	784.5404	2	819.4108	809.9158
2	857.818	848.8607	3	781.1895	771.879	3	819.2275	809.7006
3	870.5078	861.6289	4	768.4088	759.2899	4	818.9716	809.3866
4	883.1566	874.5742	5	755.6488	746.7777	5	818.6408	808.9712
5	895.7586	887.515	6	742.9193	734.3459	6	818.2323	808.451

Table S8 Q, P, and R branches for ND_3 v_2 band.

R branch at $K = 0$ (cm^{-1})			P branch at $K = 0$ (cm^{-1})			Q branch (cm^{-1})		
J	R	R’	J	P	P’	J	Q	Q’
0	759.5759	755.9911	1	738.8596	735.2591	1	749.1878	745.5891
1	770.1477	766.5948	2	728.725	725.1412	2	749.1706	745.563
2	780.8544	777.4009	3	718.7453	715.1941	3	749.0931	745.4682
3	791.6896	788.2461	4	708.924	705.4209	4	748.9552	745.3091
4	802.6466	799.2785	5	699.2644	695.8238	5	748.7566	745.0917
5	813.718	810.4373	6	689.769	686.4044	6	748.4972	744.8236

6. Absorption coefficient of $NH_{3-x}D_x$

The absorption coefficient, α_i, was determined by the following equation:

$$\alpha_i = \frac{A}{C_i \times L} \tag{S4}$$

where A, C_i, and L were the area of the peak in FTIR spectra, concentration for spices (i = $NH_{3-x}D_x$), and optical length of 8.0 m.

NH_3 absorption, α_{NH3}, was obtained by flowing 10 ppm NH_3-N_2 with 100 sccm into the cathode. The ammonia formation rate of 8.81×10^{-10} mol cm^{-2} s^{-1} was observed by HPLC, which is equivalent to 5.07 ppm in the cathode (Eq. S2). NH_3 peak area at 965 cm^{-1} in the FTIR spectra was 0.13. Therefore, α_{NH3} was 0.0032 ppm^{-1} m^{-1} (7.8×10^2 L mol^{-1} cm^{-1}), which was smaller by 18% than that of 0.0039 ppm^{-1} m^{-1} (9.5×10^2 L mol^{-1} cm^{-1}) in the previous study.[6] α_{NH2D} was determined by Eq. S5 using the FTIR data (5% H_2−95% N_2 in the cathode) at the rest potential (90 mins) and −1 V (90 mins), as shown in Fig. S4. The observed spectra included the peaks of NH_3 and NH_2D,

$$\alpha_{NH2D} = \frac{A_{NH2D}}{C_{NH2D} \times L} = \frac{A_{NH2D}}{(C_{total} - C_{NH3}) \times L} = \frac{A_{NH2D}}{(C_{total} - \frac{A_{NH3}}{\alpha_{NH3} \times L}) \times L} \tag{S5}$$

and no other peaks such as NHD_2 and ND_3 were observed.

where C_{total} was total concentration of ammonia, which was determined by HPLC. The value of α_{NH2D} was 0.0038 ppm^{-1} m^{-1} (9.2×10^2 L mol^{-1} cm^{-1}).

Next, α_{NHD2} and α_{ND3} were determined by the FTIR data (5% D_2−45%Ar −95% N_2 in the cathode) at −1 V (50, 60, 70, 80, and 90 mins), as shown in Fig. S5. The observed spectra included the peaks of NH_3, NH_2D, NHD_2 and ND_3. NH_3 and NH_2D concentrations were obtained by following procedure. α_{NHD2} and α_{ND3} were obtained by the following equation:

$$\frac{A_{ND3}}{\alpha_{ND3} \times L} + \frac{A_{NHD2}}{\alpha_{NHD2} \times L} = C_{total} - C_{NH3} - C_{NH2D} \tag{S6}$$

where C_{total} was total concentration of ammonia, which was determined by HPLC.

Eq. S6 can be written by Eq. S7:

$$A_{ND3} = -\frac{\alpha_{ND3}}{\alpha_{NHD2}} A_{NHD2} + (C_{total} - C_{NH3} - C_{NH2D}) \times L \times \alpha_{ND3} \quad \text{(S7)}$$

α_{NHD2} and α_{ND3} were 0.0037 ± 0.0019 (9.0 ± 4.6×10^2 L mol^{-1} cm^{-1}) and 0.0021 ± 0.0001 ppm^{-1} m^{-1} (5.1 ± 0.2 × 10^2 L mol^{-1} cm^{-1}), respectively.

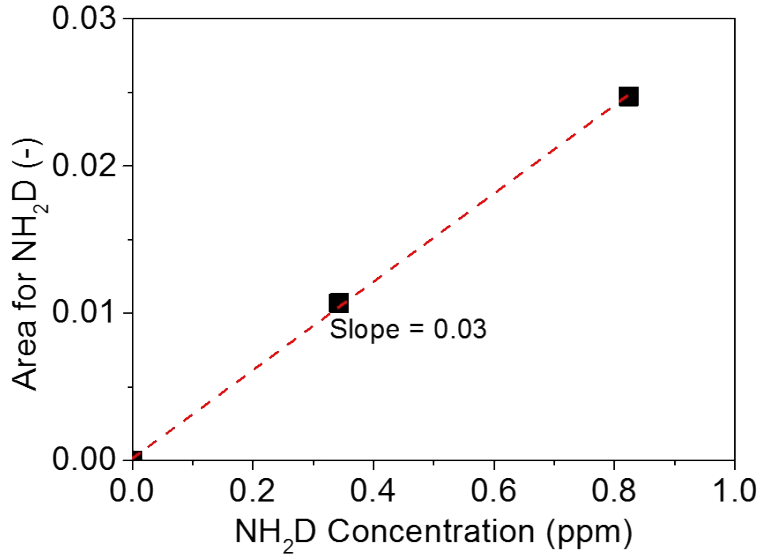

Fig. S4 Peak area of NH_2D vs. the concentration of NH_2D. The slope corresponds to $\alpha_{NH2D} \times L$.

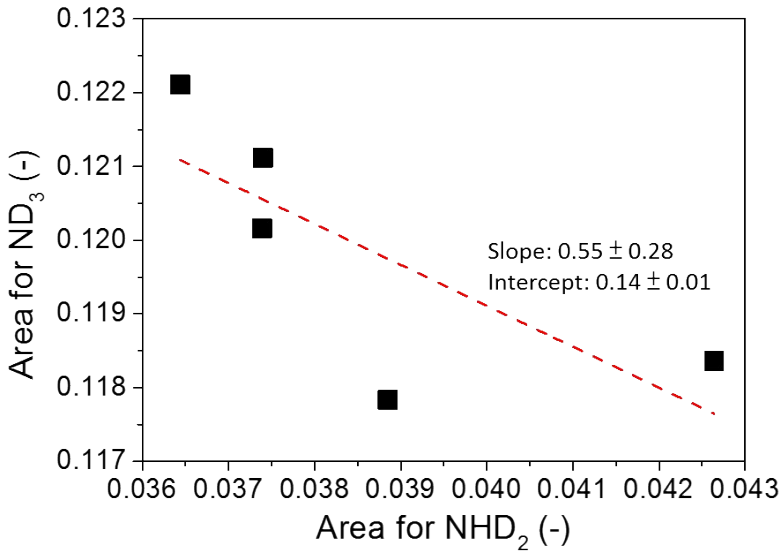

Fig. S5 The intercept was (C_{total}-C_{NH3}-C_{NH2D}) × L × α_{ND3}, and the slope corresponds to $-\alpha_{ND3}/\alpha_{NHD2}$.

7. Device for ammonia synthesis and FTIR measurement

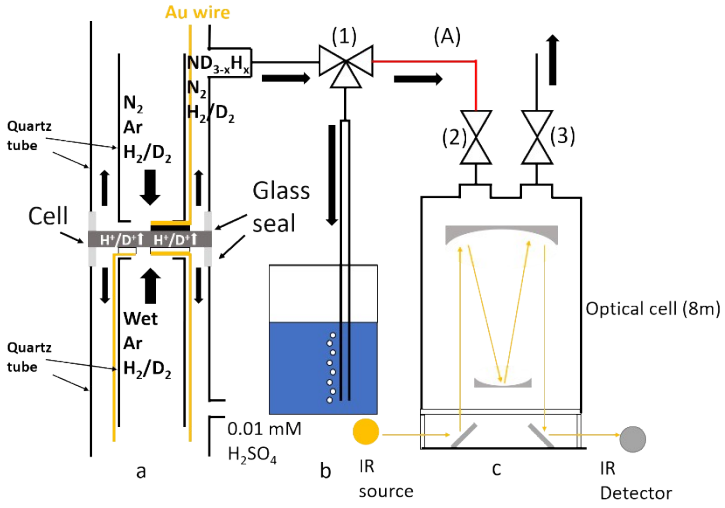

Fig. S6 Schematic image of the ammonia electrosynthesis device. (a) Ammonia electrosynthesis device. (b) Gas flow into capture solution for HPLC measurement (c) Gas flow into optical cell for FTIR analysis. The three-way valve 1 was used to control the cathode flow into the capture solution or the FTIR device. Valves 2 and 3 are switches for the gas inlet and outlet, respectively, of the optical cell. (A) The influence of gas line temperature on NH_3 concentration was discussed in section 15.

8. H^+ (or D^+) diffusion through the electrolyte at the rest potential

Proton diffusion from the anode to the cathode is caused by the driving force of H_2 concentration gradient. At the steady state, the proton flux, J_H, is a constant, which can be described by Eq. S8.

$$J_H = -D_H \frac{\partial c_{H2}}{\partial x} \quad \text{(S8)}$$

Because $\frac{\partial J_H}{\partial t} = 0$ at the steady state, Eq. S8 can be written as Eq. S9:

$$J_H = -D_H \frac{c_{H2,anode} - c_{H2,cathode}}{L} \quad \text{(S9)}$$

where D_H, c_{H2}, $c_{H2,anode}$, $c_{H2,cathode}$, and L are the diffusion coefficient for H^+ in $BaCe_{0.9}Y_{0.1}O_{3-\delta}$ (BCY), H_2 concentration, H_2 concentration in the anode, H_2 concentration in the cathode, and the thickness of BCY electrolyte, respectively. For the operation condition of 10% H_2−90% Ar in the anode and 5% D_2−45% Ar−50% N_2, the parameters were summarized in Table S9.

Table S9 Parameters for calculation the H^+ flux

D_H (m^2 s^{-1})[7]	$c_{H2,\ anode}$ (mol l^{-1})	$c_{H2,cathode}$ (mol l^{-1})	L (mm)
1.0×10^{-9}	0.00148	0	0.08

J_H is about 1.86×10^{-10} mol cm^{-2} s^{-1}. The H_2 partial pressure, p_{H2}, in the cathode was obtained by Eq. S10.

$$p_{H2} = \frac{J_H \times A \times R \times T}{f} \quad \text{(S10)}$$

where A, R, T, and f are the electrode area, gas constant, temperature, and flow rate.

The same calculation was conducted for the operation condition of 10% D_2−90% Ar in the anode and 5% H_2−95% N_2 in the cathode. The diffusion coefficient for deuterium in BCY, D_D, is described by Eq. S11.

$$D_D = \frac{D_H}{\sqrt{2}} \quad \text{(S11)}$$

The parameters were summarized in Table S10.

Table S10 Parameters for calculation the D^+ flux

D_D (m^2 s^{-1})	$c_{D2,\ anode}$ (mol l^{-1})	$c_{D2,cathode}$ (mol l^{-1})	L (mm)
7.1×10^{-9}	0.00148	0	0.08

Here, D_H, $c_{H2,anode}$, $c_{H2,cathode}$ are the diffusion coefficient for D^+ in BCY, D_2 concentration in the anode, and D_2 concentration in the cathode, respectively.

J_D is about 1.31×10^{-10} mol cm^{-2} s^{-1}. D_2 partial pressure, p_{D2}, in the cathode was also obtained by Eq. S10.

9. Decomposition behavior of ammonia species

The decomposition behavior of ammonia species was examined. As described in the main text, the valves 1, 2, and 3 (see Fig. S6) were closed to examine the influence of the optical cell on the concentration of ammonia product (i.e., the adsorption or decomposition of ammonia), as shown in Fig. S7, the intensities of the ND_3 peaks monotonously decreased with elapsed time, whereas the intensities of the NH_3, NH_2D, and NHD_2 peaks did not change with elapsed time. Thus, the decrease in the ND_3 concentration was caused by the decomposition rather than the exchange reaction of ND_3 and H_2O to form $NH_{3-x}D_x$ in the optical cell. The decomposition rate was about 0.4% per min based on the result in the stage 3, and the space time in the optical cell was 5 min in the stage 2, considering the current condition (the total gas flow rate in the cathode:100 sccm; the volume of the optical cell: 500 cm^3). Therefore, the decomposition rate in the space time was around 2% in the stage 2, which can be negligible in our experiments.

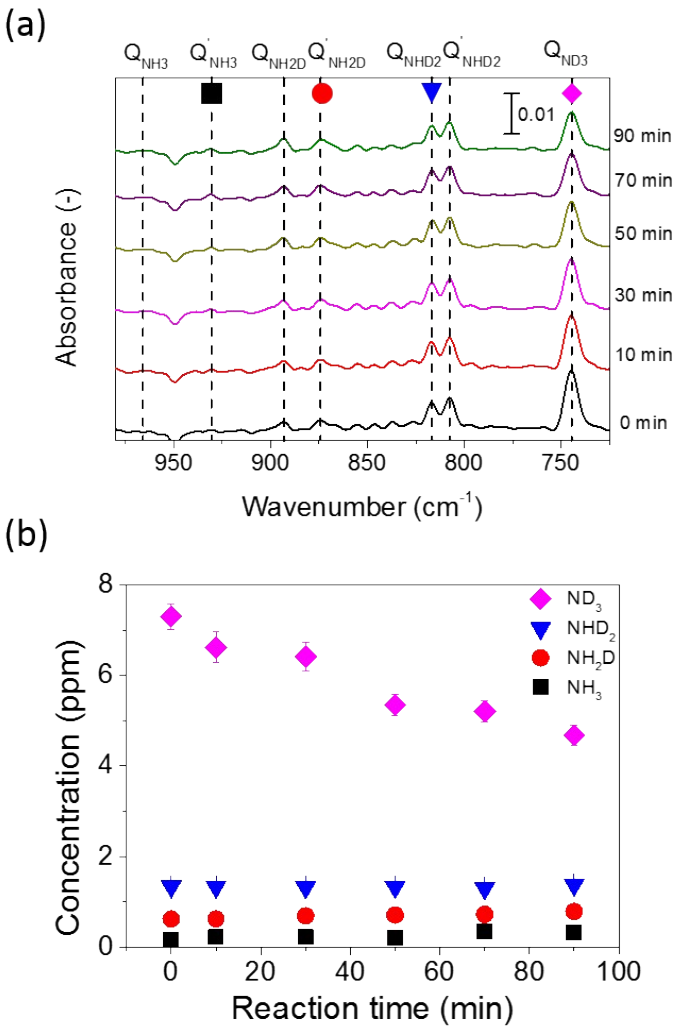

Fig. S7 (a) was FTIR spectra of ammonia products using porous pure Fe in 5% D_2−45% Ar−50% N_2 with three valves closed. (b) shows the concentrations of the $NH_{3-x}D_x$ peaks in (a).

10. Deconvolution of the spectrum involving NH_2D Q' branch and NH_3 P

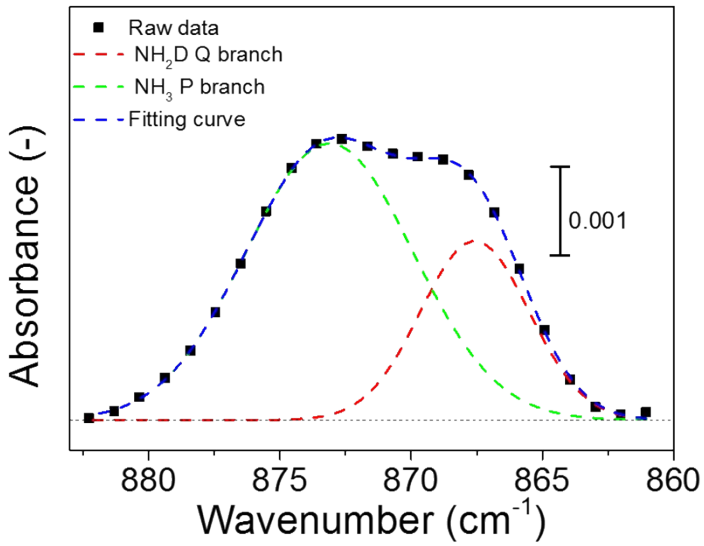

Fig. S8 Deconvolution of the spectrum involving NH_2D Q' branch and NH_3 P branch. The spectrum was observed at −1 V and 550 °C in 5% H_2−95% N_2 in the cathode. The spectrum was observed at 90 min after applying the voltage.

11. FTIR spectra of the ammonia products

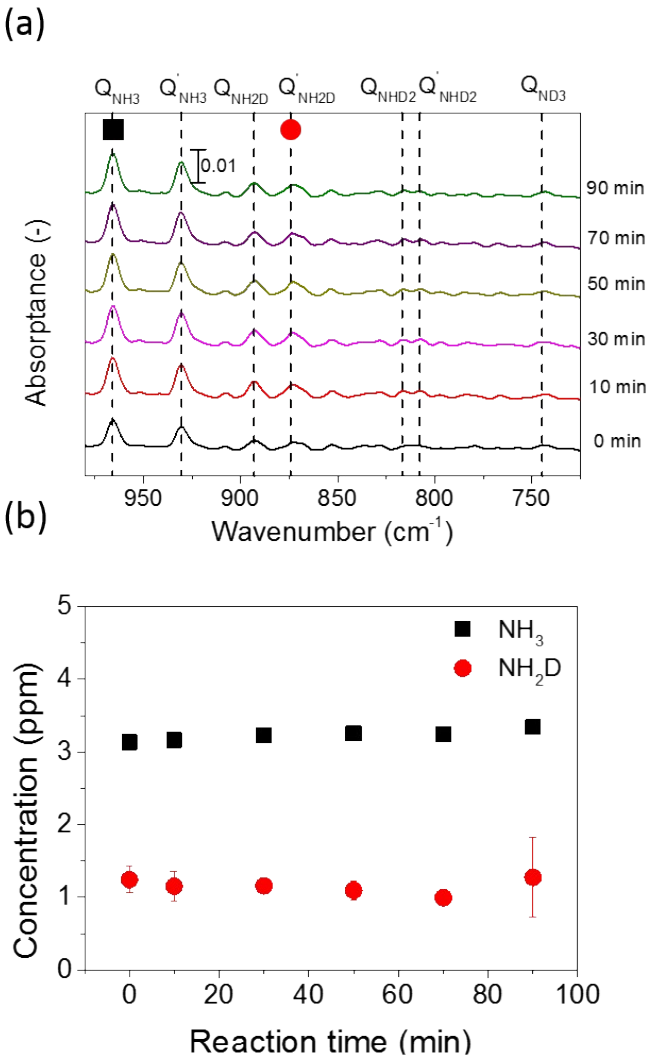

Fig. S9 (a) was FTIR spectra of the ammonia products using porous pure Fe in 5% H_2−95% N_2 with three valves closed. (b) showed the concentrations of the $NH_{3-x}D_x$ peaks in (a).

12. Cell shape and the equipment for ammonia formation and FTIR

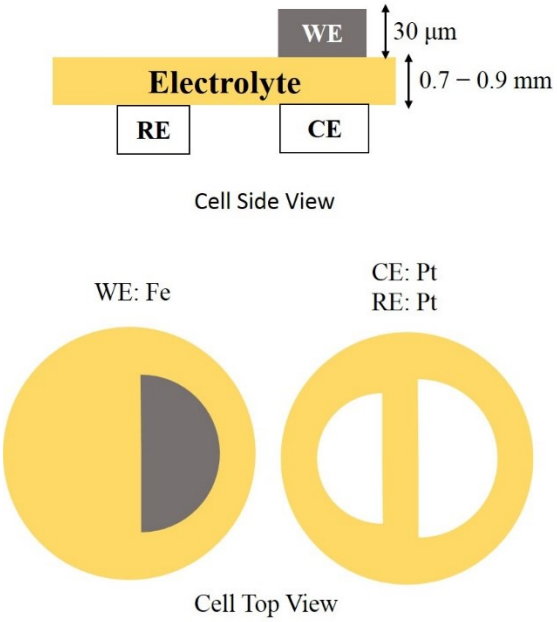

Fig. S10 Schematic images of a single cell (working electrode (WE) is porous pure Fe, and counter electrode (CE) and reference electrode (RE) are platinum (Pt).)

13. Experimental conditions for ammonia electrochemical synthesis

Table S11 Reaction conditions in the experiment for the electrochemical promotion of ammonia formation and deuterium isotope analysis.

	Flow rate (sccm)	Cathode atmosphere	Flow rate (sccm)	Anode atmosphere
Electrochemical promotion of ammonia formation detected by HPLC	40	H_2−N_2−Ar	30	H_2−H_2O−Ar
Deuterium isotope analysis by FTIR	100	D_2−N_2−Ar or H_2−N_2	30	H_2−H_2O−Ar or wet D_2−Ar

14. Protocol for the benchmarking of electrochemical nitrogen reduction

A protocol for benchmarking of ammonia electrochemical synthesis is summarized in Table S12.

1. To check the accuracy of present ammonia electrochemical measurements, blank tests were conducted in pure N_2 (purity: 99.9999%) or pure Ar (purity: 99.99%), according to the following protocol, which is described in sections 16 and 17 in detail.

2. The influence of Ar purity (99.99% and 99.9999%) on ammonia formation rate in a gaseous mixture of H_2−N_2−Ar was examined in section 18.

2'. The ammonia formation rate in a gaseous mixture of Ar (purity: 99.99%)−H_2 (purity: 99.99%) was also examined. No ammonia formation was observed.

3. FTIR and HPLC detection limits were also determined in sections 16 and 17.

4. The influence of gas-line temperature on the NH_3 concentration was tested in section 15.

5. Stability test for composition and concentration of $NH_{3-x}D_x$ were examined in Fig. S7 and Fig. S9 to check the changes of $NH_{3-x}D_x$ in an optical cell with elapsed time.

Table S12 Protocol for the benchmarking of ammonia electrochemical synthesis.

1. Blank test	HPLC	Section 16
	FTIR	Section 17
2. Ar purity	HPLC	Section 18
3. Detection limit	HPLC	Section 16
	FTIR	Section 17
4. Gas line temperature	The influence of gas tube temperature on the NH_3 partial pressure	Section 15
5. Stability test	8 m-optical cell	Fig. S7 and Fig. S9

15. Influence of gas line temperature on ammonia concentration

Fig. S11 shows detected NH_3 concentration with 10 ppm NH_3−N_2 flow into the optical cell at different gas-line temperatures. The result showed that the NH_3 concentration kept constant around at 10 ppm when the gas-line temperature changed from 80°C to 160°C, which indicates that the influence of gas line temperature on ammonia concentration can be negligible.

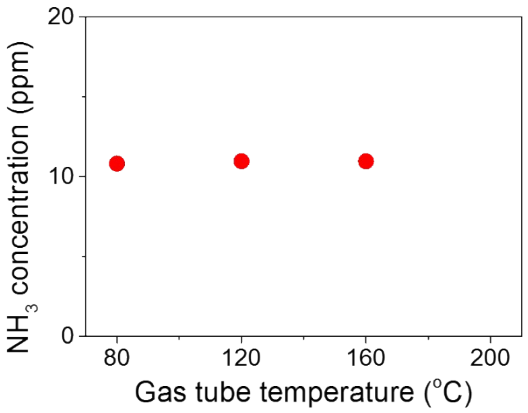

Fig. S11 The relationship between the gas-line temperature and ammonia concentration in the optical cell.

16. Blank test for ammonia formation using HPLC in pure N_2 and Ar

As blank tests, ammonia formation rates were measured in pure Ar and N_2 with cathodic polarization using porous pure Fe cathode at 550°C, as shown in Fig. S12. The detection limit of ammonia formation rate was around 2×10^{-12} mol cm^{-2} s^{-1} for HPLC, and the observed ammonia formation rates were below 2×10^{-12} mol cm^{-2} s^{-1}. Based on the results, we concluded almost no

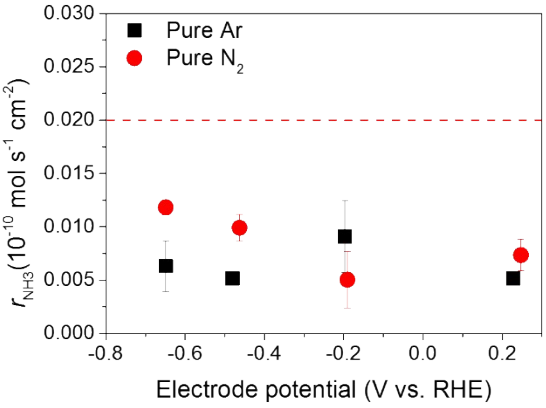

Fig. S12 Ammonia formation rates in pure Ar and pure N_2 at 550°C. The red broken line is the detection limit of HPLC.

ammonia formation in pure N_2 and Ar.

17. Blank test for ammonia formation using FTIR in pure Ar and pure N_2 with an 8 m-optical cell

As blank tests, FTIR spectra were measured at 550°C in pure Ar and N_2 at OCV and –1 V, respectively, as shown in Fig. S13. 10% H_2–90% Ar was introduced into the anode. The result showed that no peaks of the compositions of NH_3 were observed. The background noise of the absorbance is around ±0.00025 between 900 and 1000 cm^{-1}. Based on the background noise, the NH_3 peak height of 0.001 is the detection limit, which corresponds to the NH_3 concentration of 0.2 ppm.

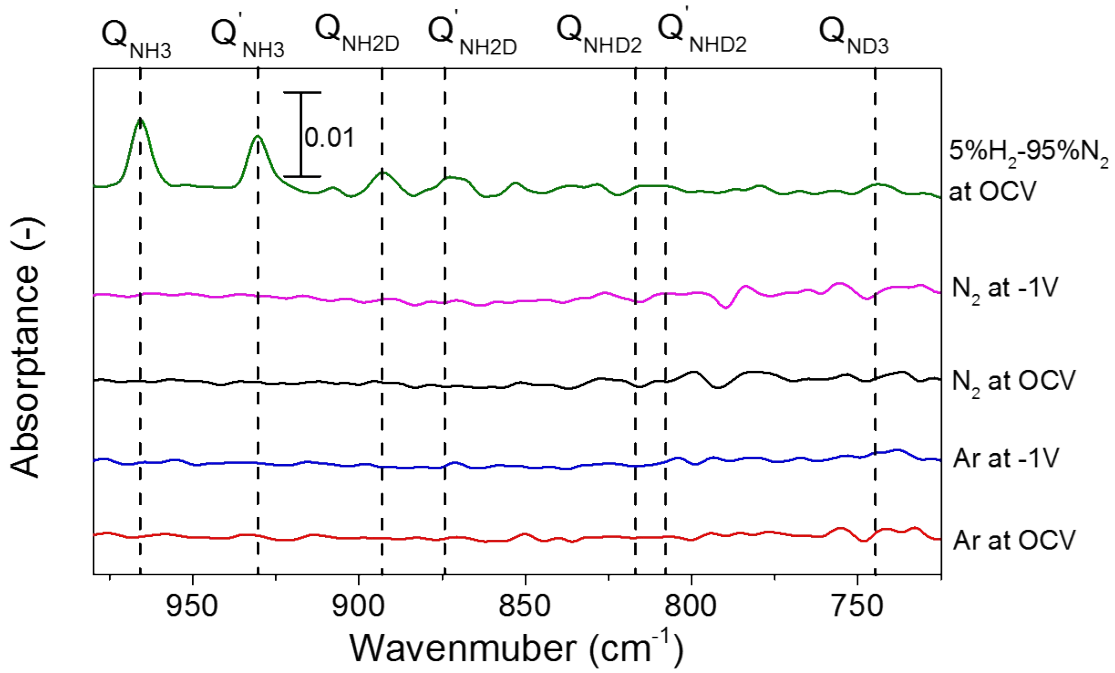

Fig. S13 FTIR spectra after reaction time of 90 min in N_2 and Ar at OCV and –1V.

18. The effect of Ar purity on ammonia formation rate

Fig. S14 shows the ammonia formation rate at 550°C and 10% H_2−40% Ar−50% N_2 using Fe cathode with different Ar purity (99.99% and 99.9999%). The result shows that the ammonia formation rate does not change with different Ar purity.

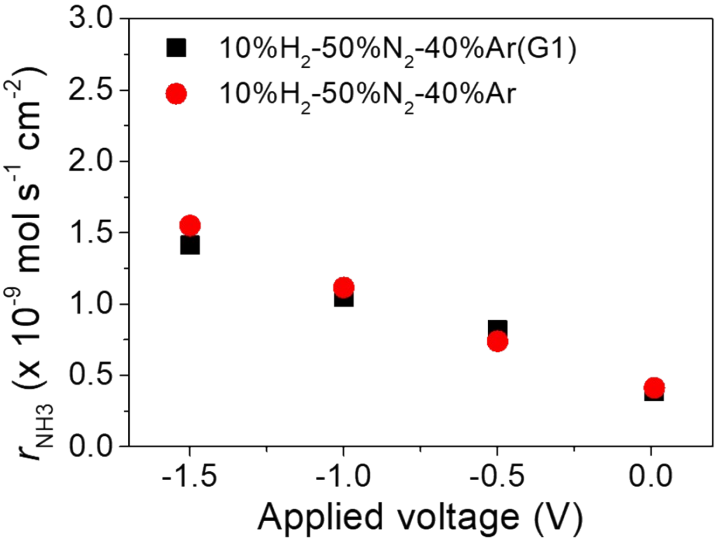

Fig. S14 Ammonia formation rate with Ar purity 99.9999% (black square) and purity 99.99% (red circle) at 550°C using Fe cathode.

References

1. C. W. David, *Journal of Chemical Education,* **73** (1), 46−50 (1996).
2. S. Urban and D. Papousek, *Journal of Molecular Spectroscopy,* **101** 1−15 (1983).
3. V. A. Job, S. B. Kartha, K. Singh, and V. B. Kartha, *Journal of Molecular Spectroscopy,* **126** 290−306 (1987).
4. V. M. Devi, P. P. Das, and K. N. Rao, *Journal of Molecular Spectroscopy,* **88** 293−299 (1981).
5. S. B. Kartha, K. Singh, V. A. Job, and V. B. Kartha, *Journal of Molecular Spectroscopy,* **129** 86−98 (1988).
6. G. Laroche, J. Vallade, R. Bazinette, P. v. Nijnatten, E. Hernandez, G. Hernandez, and F. Massines, *Revuw of scientific instrumnt,* **83** 103508 (2012).
7. S. Zhuang, N. Han, Q. Zou, S. Zhang, and F. Song, *Membranes,* **10** (8), 164 (2020).